Effects of milling, doping and cycling of NaAlH$_4$ studied by vibrational spectroscopy and X-ray diffraction

S. Gomes[a], G. Renaudin[a], H. Hagemann[b], K. Yvon[a,*], M.P. Sulic[c], C.M. Jensen[c]

[a] *Laboratoire de Cristallographie, Université de Genève, 24 quai E. Ansermet, CH-1211 Geneva 4, Switzerland*
[b] *Département de Chimie Physique, Université de Genève, 30 quai E. Ansermet, CH-1211 Geneva 4, Switzerland*
[c] *Department of Chemistry, University of Hawaii, Honolulu, HI 96822, USA*

Abstract

The effects of milling and doping NaAlH$_4$ with TiCl$_3$, TiF$_3$ and Ti(OBu^n)$_4$, and of cycling doped NaAlH$_4$ have been investigated by infrared (IR) and Raman spectroscopy and X-ray powder diffraction. Milling and doping produce similar effects. Both decrease the crystal domain size ($\sim$900 Å for milled and $\sim$700 Å for doped, as compared to $\sim$1600 Å for unmilled and undoped NaAlH$_4$) and increase anisotropic strain (by a factor >2.5, mainly along c). They also influence structure parameters such as the axial ratio c/a, cell volume and atomic displacement amplitudes. They show IR line shifts by $\sim$15 cm^{-1} to higher frequencies for the Al–H asymmetric stretching mode ν_3, and by $\sim$20 cm^{-1} to lower frequencies for one part of the H–Al–H asymmetric bending mode ν_4, thus suggesting structural changes in the local environment of the [AlH$_4$]$^-$ units. The broad ν_3 bands become sharpened which suggests a more homogeneous local environment of the [AlH$_4$]$^-$ units, and there appears a new vibration at 710 cm^{-1}. The Raman data show no such effects. Cycling leads to an increase in domain size (1200–1600 Å), IR shifts similar to doped samples (except for TiF$_3$: downward shift by $\sim$10 cm^{-1}) and a general broadening of the ν_3 mode that depend on the nature of the dopants. These observations support the idea that some Ti diffusion and substitution into the alanate lattice does occur, in particular during cycling, and that this provides the mechanism through which Ti-doping enhances kinetics during re-crystallisation.
© 2004 Elsevier B.V. All rights reserved.

Keywords: Hydrogen storage materials; Infrared and Raman spectroscopy; X-ray diffraction; Alanates

1. Introduction

Doping of sodium tetrahydrido aluminate (NaAlH$_4$) with titanium based catalysts such as Ti(OBu^n)$_4$, TiCl$_3$ and TiF$_3$ improves its hydrogen release properties [1–6]. The doping process usually consists of milling the alanate in the presence of few mole percent of catalysts. However, several studies indicate that milling NaAlH$_4$ in the absence of catalysts also improves hydrogen release [7–9]. Furthermore, there appears to exist an optimum milling time to introduce the dopant into the hydride, extended milling times leading to a spontaneous

hydrogen loss [9]. Up to now, the mechanism of action of the Ti dopants has not been established. In particular, the location of titanium dopants has been a subject of a great deal of speculation and controversy. One school of thought has held that the remarkable enhancement of the hydrogen cycling kinetics in Ti doped NaAlH$_4$ is due to surface-localized catalytic species consisting of elemental titanium or a Ti–Al alloy [1,4,6,10]. Alternatively, it has been hypothesized that doping involves the substitution of titanium into the bulk of the hydride [11–13]. The present work represents an attempt to measure possible structural and microstructural changes in NaAlH$_4$ induced by milling, doping and cycling. For this purpose various samples of untreated, doped, milled and cycled hydrides and deuterides were investigated by using

---

* Corresponding author. Tel.: +41 22 379 62 31; fax: +41 22 379 68 64.
  E-mail address: klaus.yvon@cryst.unige.ch (K. Yvon).

vibration spectroscopy (IR and Raman) and X-ray powder diffraction.

2. Experimental

2.1. Preparation, milling, doping and cycling

Sodium aluminium hydride was obtained from Albemarle Corp. and recrystallized from tetrahydrofuran prior to use (samples 1–3 called "pure", see experiment Nos. 1–4 in Tables 1 and 4). The deuteride $NaAlD_4$ (>99% D, sample 4, see experiment No. 5 in Table 1) was synthesized by the literature method [14]. X-ray powder diffraction (XPD) analysis (see Table 1) indicated that the hydride samples were single phase while the deuteride sample contained ~5 wt.% NaF and ~25 wt.% metallic Al. Milling was performed by grinding the pure hydride and deuteride samples 2 and 4, respectively, in a ceramic mortar during 20 and 40 min in an argon filled glove-box (called "milled" samples thereafter, see experiment Nos. 6–9 in Tables 1 and 4). XPD analysis showed that these samples contained no new phases. Doping was performed by ball-milling the pure hydride samples 1 and 3 in the presence of $Ti(OBu^n)_4$ (2 and 6 mol%, Aldrich, purity 97%), $TiCl_3$ (2 mol%, Aldrich, purity 99.999%) and TiF_3 (6 mol%, Aldrich, purity 99%) as described in [2,15]. XPD analysis on these samples (called "doped" samples thereafter, see experiment Nos. 11–13 in Tables 1 and 4) revealed the presence of metallic Al (up to 7 wt.%) and TiF_3 (1 wt.%) for one doped sample (experiment No. 13). Cycling was performed on the 2 mol% doped sample 3 according to a dehydrogenation by heating at 160 °C for 5 h and a rehydrogenation upon standing under 100 bar of H_2 at 100 °C for 12 h (with three successive cycles). XPD analysis on these samples (called "cycled" samples thereafter, see experiment Nos. 14–16 in Tables 1 and 4) indicated the presence of the decomposition products Na_3AlH_6 (up to 35 wt.%), metallic Al (up to 12 wt.%) and NaCl (5 wt.%). Given the scarcity of spectroscopy literature on sodium hexahydrido-aluminate (only one reported Raman spectrum [16]) the compound was synthesized by the method of Huot et al. [17] and investigated by IR and Raman spectroscopy. The sample contained about 5 wt.% of NaH impurity. All measurements were performed within less than 1 month after sample preparation. Measurements performed a few months later confirmed that the samples changed their phase compositions over time, in particular the cycled ones for which the Na_3AlH_6 phase disappeared at the expense of metallic Al.

2.2. Raman and infrared spectroscopy

The Raman set-up used was the same as that described previously [18,19]. It consisted of an Argon ion laser (488 nm excitation wavelength) and a Kaiser Optical Holospec monochromator equipped with a liquid nitrogen cooled CCD camera. The spectral resolution was ~3–4 cm^{-1}.

Additional measurements were performed by using a Labram Raman microscope using 532 nm excitation. The samples were enclosed in sealed glass capillaries with a diameter Ø 1.0 mm by using a purified Ar filled glove-box. The Fourier transformation infrared (FT-IR) spectrometer used was a Paragon 1000 (Perkin-Elmer) equipped in attenuated total reflection (ATR) mode with the Golden Gate Single Reflection Diamond (P/N 10500 Graseby-Specac Series). The diamond crystal had a refractive index of 2.4 at 1000 cm^{-1}. The spectral resolution was 4 cm^{-1} and the spectral range 500–4400 cm^{-1}. The powder samples were pressed against the crystal with a calibrated strength in a purified Ar filled glove-box and protected by an airtight polyethylene film during measurement. Additional measurements in nujol suspension (prepared in a purified Ar filled glove-box and placed between two airtight NaCl plates) were done using a Bio-Rad Excalibur instrument, and KBr pellets (hand pressed in an inert atmosphere) using a Nicolet Nexus 470 FT-IR instrument. All spectra were recorded at room temperature. Both the Raman and infrared spectra were analysed by using the line fitting procedure with Lorentzian profile of the program SPECTRAW [20]. It should be noted that the Raman intensities observed for Na_3AlH_6 were much weaker than those for $NaAlH_4$.

2.3. X-ray powder diffraction (equipment and analysis)

The samples were analysed on a Huber Guinier Diffractometer 600 by using monochromatic Ge(1 1 1) Cu Kα_1 radiation. The system was equipped with a closed-cycle helium Helix Model 22 Refrigerator. The powders were mixed with an internal silicon standard and placed between two polyethylene terephtalate foils (Goodfellow) of 0.013 mm thickness. All manipulations were performed in a purified Ar filled glove-box. In view of the instability of the samples (especially the doped and cycled ones) and the long data acquisition times (>12 h) all measurements except one (experiment No. 4) were performed at 10 K (diffraction interval $10° < 2\theta < 100°$, step size $\Delta 2\theta = 0.02°$, counting time per step 10 s). Samples 1–3 were studied in order to check the reproducibility of the microstructural analysis, and one of these (sample 3) was investigated at room temperature in order to check if microstructural properties such as strain were intrinsic to the $NaAlH_4$ phase and not induced during cooling (experiment Nos. 3–4). The following microstructure parameters were extracted from the data by conventional Rietveld analyses (program Fullprof.2k [21]): average crystallite size and anisotropic strain from diffraction line broadening, and peak shift parameter Sh (related to stacking faults [21–23]) from the displacements of certain groups of reflections (see below). The diffraction profiles (both instrumental and sample intrinsic) were modelled by using a Thomson–Cox–Hastings pseudo-Voigt function [21] (convolutions between Gaussian and Lorentzian components having different full widths at half maximum, FWHM) to simulate the peak shapes of both $NaAlH_4$, Si and impurities phases when present. Structural

Table 1

Results of XPD analyses on pure, milled, doped and cycled alanate samples; strain anisotropy along c; pure $NaAlH_4$ refers to unmilled and undoped as-received samples; e.s.d.'s in parentheses

Experiment		Sample		Phase analysis	Structure analysis		Microstructure analysis		
No.	Temperature (K)	Sample	Treatment	Composition (wt.%)	c/a, V (Å³)	Atomic displacements B_{Na} (Å²), B_{Al} (Å²)	Grain size (Å)	Strain (‰), anisotropy	Shift parameter Sh for (h,k,l), $l = 4n$
Pure alanates									
1	10	1	$NaAlH_4$, untreated	$NaAlH_4$ single phase	2.24231 (3), 279.116 (4)	4.08 (8), 3.77 (6)	1597 (1)	0.594, 0.062	−0.20 (2)
2	10	2	$NaAlH_4$, untreated	$NaAlH_4$ single phase	2.24222 (3), 279.258 (3)	4.37 (7), 3.87 (4)	1705 (1)	0.590, 0.142	−0.55 (2)
3	10	3	$NaAlH_4$, untreated	$NaAlH_4$ single phase	2.24239 (3), 279.142 (4)	4.17 (8), 3.92 (6)	1828 (1)	0.544, 0.128	0.07 (2)
4	295	3	$NaAlH_4$, untreated	$NaAlH_4$ single phase	2.25947 (3), 286.567 (3)	5.81 (7), 4.76 (5)	1770 (2)	0.439, 0.051	0.04 (2)
5	10	4	$NaAlD_4$, untreated	68 wt.% $NaAlD_4$, 27 wt.% Al, 5 wt.% NaF	2.24060 (8), 276.415 (7)	4.3 (2), 4.6 (1)	1038 (1)	0.883, 0.177	0.06 (4)
Milled alanates									
6	10	2	Milled 20 min	$NaAlH_4$ single phase	2.24315 (6), 279.228 (6)	4.7 (1), 4.25 (7)	918 (1)	1.676, 0.130	−0.07 (3)
7	10	2	Milled 40 min	$NaAlH_4$ single phase	2.24895 (9), 279.546 (8)	5.1 (1), 4.1 (1)	801 (1)	2.158, 0.255	0.19 (5)
8	10	4	Milled 20 min	68 wt.% $NaAlD_4$, 27 wt.% Al, 5 wt.% NaF	2.24114 (9), 276.394 (9)	5.0 (1), 4.6 (1)	767 (1)	1.587, 0.157	0.07 (5)
9	10	4	Milled 40 min	67 wt.% $NaAlD_4$, 28 wt.% Al, 5 wt.% NaF	2.2472 (2), 276.79 (2)	5.6 (3), 4.9 (2)	608 (1)	2.234, 0.459	−0.11 (6)
Doped alanates									
11	10	1	Doped, 6 mol% $Ti(OBu^n)_4$	$NaAlH_4$ single phase	2.24320 (6), 278.925 (6)	4.7 (1), 4.3 (1)	594 (1)	1.807, 0.105	−0.04 (4)
12	10	3	Doped, 2 mol% $TiCl_3$	93 wt.% $NaAlH_4$, 7 wt.% Al	2.24365 (6), 279.268 (6)	4.8 (1), 4.42 (7)	759 (1)	1.614, 0.249	−0.22 (3)
13	10	1	Doped, 6 mol% TiF_3	97 wt.% $NaAlH_4$, 2 wt.% Al, 1 wt.% TiF_3	2.24349 (8), 279.355 (9)	5.1 (2), 4.4 (1)	698 (1)	1.705, 0.185	−0.08 (5)
Cycled alanates									
14	10	3	Cycled, 2 mol% $Ti(OBu^n)_4$	56 wt.% $NaAlH_4$, 9 wt.% Al, 35 wt.% Na_3AlH_6	2.24295 (7), 279.130 (6)	3.1 (1), 6.1 (2)	1230 (2)	1.503, 0.091	−0.47 (3)
15	10	3	Cycled, 2 mol% $TiCl_3$	72 wt.% $NaAlH_4$, 12 wt.% Al, 11 wt.% Na_3AlH_6, 5 wt.% NaCl	2.24463 (6), 279.616 (6)	5.0 (1), 4.05 (7)	1124 (1)	0.931, 0.468	−0.35 (4)
16	10	3	Cycled, 2 mol% TiF_3	76 wt.% $NaAlH_4$, 9 wt.% Al, 15 wt.% Na_3AlH_6	2.24438 (5), 279.633 (5)	4.6 (1), 4.26 (7)	1606 (1)	1.601, 0.352	−0.09 (3)

parameters of the alanate structure were fixed at the values reported by Hauback et al. [24]: space group $I4_1/a$, Na in 4*a* (0, 1/4, 1/8), Al in 4*b* (0, 1/4, 5/8) and H in 16*f* (0.2372, 0.3836, 0.5469). This procedure was justified because subsequent refinements on milled, doped and cycled samples gave no evidence for significant changes in atom positions. The deconvolution by FullProf.2k allowed extracting the intrinsic line profile from the observed one provided the instrumental resolution function is known (from the adding of internal Si in each sample). Any increase of FWHM in the observed diffraction profile with respect to the instrumental FWHM was considered to be intrinsic to the sample. Isotropic average crystallite size and anisotropic strain effects were then separated and refined due to the distinct angular dependences of the Lorentzian and Gaussian components of the intrinsic line broadening. All samples have shown strain mainly directed along *c*. The peak shift parameter Sh was refined according to the expression $2\theta_{\text{shifted}} = 2\theta_{\text{Bragg}} + 2\text{Sh}\,d^2\tan\theta \times 10^{-2}$ for reflections (*h*,*k*,*l*) with $l = 4n$. Although some values obtained during this work clearly differed from zero and thus provided evidence for the existence of stacking faults [21–23] this parameters will not be discussed in the text. The results (cell parameters, atomic displacement parameters, grain size, strain, Sh parameter) are summarized in Table 1.

3. Results and discussion

3.1. Pure NaAlH₄ and NaAlD₄

3.1.1. Structure

The cell parameters at 10 K and room temperature are consistent with those reported in previous work [11,14,24–28]. However, they show small but significant differences among the samples (up to 30 e.s.d.'s) that presumably reflect effects due to the sample preparation. For the hydride samples the cell volumes at 10 K vary between $V = 279.12$ (No. 1) and $279.26\,\text{Å}^3$ (No. 2) while the axial ratios vary between $c/a = 2.2422$ (No. 2) and 2.2424 (No. 3). The latter are bigger than for the deuteride sample (No. 5: $c/a = 2.2406$) and tend to increase with temperature (No. 4: $c/a = 2.2595$ at 295 K), i.e. the lattice expands mainly along *c*. As to the metal atom displacements they are clearly overestimated ($B_{\text{Na}} = 4.1$–$4.4\,\text{Å}^2$, $B_{\text{Al}} = 3.8$–$3.9\,\text{Å}^2$) but their relative values ($B_{\text{Na}} > B_{\text{Al}}$) are consistent with those reported (except for 8 K neutron data $B_{\text{Na}} < B_{\text{Al}}$ [24]) and increase as expected with temperature. The microstructural parameters change only little as a function of temperature. The average grain size of sample 3, for example, is slightly bigger at 10 K (1828 Å) than at room temperature (1770 Å), and its strain measured at 10 K (average value of 0.54‰ with an anisotropy of 0.13‰ mainly along *c*) is slightly bigger than that measured before at room temperature (average value of 0.44 ‰ with an anisotropy of 0.05‰). This suggests that cooling increases slightly strain and anisotropy. No literature data are available for comparison.
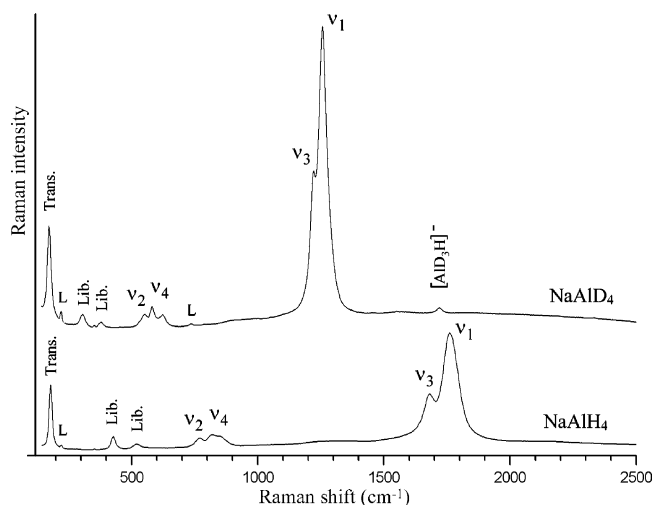

Fig. 1. Raman spectra at room temperature of NaAlH₄ and NaAlD₄. Lines labelled L are Laser plasma lines not belonging to the Raman spectrum; 'Trans.' and 'Lib.' indicate translation and libration modes, respectively.

3.1.2. Vibrations

The Raman and IR spectra are shown in Figs. 1 and 2, respectively, and compared with literature data on NaAlH₄ [29–33] and NaAlD₄ [30] in Tables 2 and 3. The Raman spectra of the hydride agree with those reported [29–32]. Those of deuteride reveal the expected isotope frequency shifts for the internal $[\text{AlD}_4]^-$ vibrations. The shifts for the external vibrations confirm recent [29] and previous assignments [31] to librational (429 and 521 cm^{-1}) and translational (180 cm^{-1}) modes. In addition, a weak band occurs at 1719 cm^{-1} that can be assigned to the Al–H stretching mode in a $[\text{AlD}_3\text{H}]^-$ moiety, indicating the presence of ca. 1–2% hydrogen impurity (relative to deuterium) in the deuterated sample. The occurrence of a single band in this region indicates the presence of a single Al−H bond length which is in agreement with the structural description of the $[\text{AlH}_4]^-$ moiety by a flattened tetrahedral polyhedron having S₄ site symmetry and a single H site [24].

The IR spectra are shown in Fig. 2 and the observed frequencies are collected in Table 3. All pure untreated samples gave exactly the same spectra (for this reason no indication about sample number are given). They are similar for preparations in KBr pellets and nujol mulls and agree with literature data [31–33]. The stretching bands around 1700 cm^{-1} are extremely broad (about 270 cm^{-1} with a large shoulder at the left). While their maximum can be assigned to the ν_3 $[\text{AlH}_4]^-$ asymmetric stretching band one should be aware that the spectra in this region may be complicated by a series of possible contributions. There are site and factor group splittings: the degenerate ν_3 mode of F_2 symmetry for the free ion (point group T_d) is split into $B + E$ contributions (site group S₄) which transform as $A_u + B_g + E_g + E_u$ in C₄ₕ (factor group of the crystal). In addition, by analogy with observations for the analogous $[\text{BH}_4]^-$ ion [34], one can expect the presence of Fermi resonances involving overtones and combination bands of the lower frequency modes observed
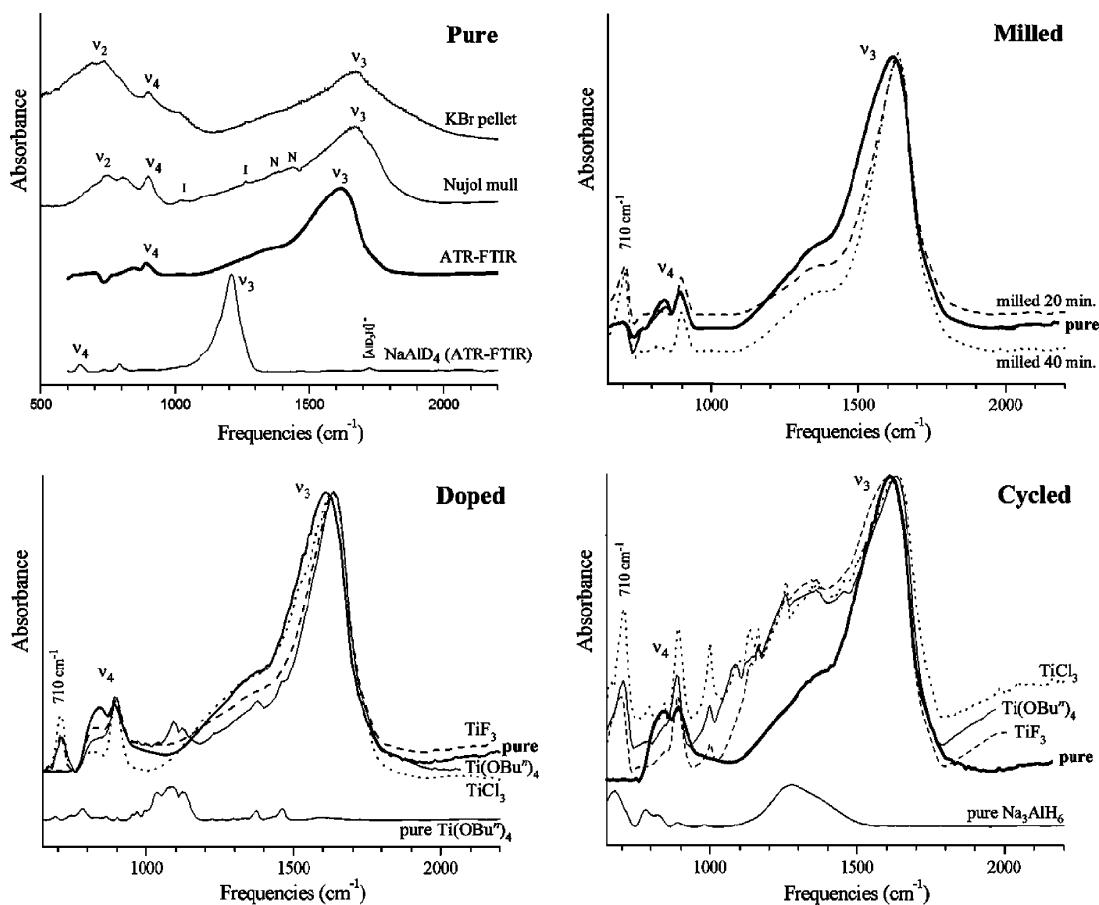
Fig. 2. Infrared spectra at room temperature. Top left: pure NaAlH$_4$ from different infrared spectrometers and comparison with NaAlD$_4$. Top right: milled NaAlH$_4$ (experiment Nos. 1, 6 and 7, ATR FT-IR mode). Bottom left: NaAlH$_4$ doped with various Ti-catalysts (experiment Nos. 1, 10–13, ATR FT-IR mode) and comparison with pure Ti(OBu^n)$_4$. Samples doped with 2 and 6 mol% Ti(OBu^n)$_4$ show the same spectra. Bottom right: cycled NaAlH$_4$ doped with various Ti-catalysts (experiment Nos. 1, 14–16, ATR FT-IR mode) and comparison with pure Na$_3$AlH$_6$.

Table 2
Raman frequencies (ω_i in cm^{-1}) of pure NaAlH$_4$ (sample 1) and NaAlD$_4$ (sample 4) at room temperature; ratio ω_i^H/ω_i^D calculated from data of this work (estimated errors ±2 cm^{-1})

ω_i	Pure NaAlH$_4$					Pure NaAlD$_4$		Ratio (ω_i^H/ω_i^D)
	[29]	[32]	[31]	[30]	This work	[30]	This work	
Translation	107	–	117	–	–			
	116	–	126	–	–			
	174	–	182	–	180		174	1.03
Libration	419	–	427	–	429	–	306	1.40
	511	–	520	–	521	–	379	1.37
ν_2	765	767	767	–	770	–	550	1.40
ν_4	812	824	816	772	817	572	582	1.40
	847	–	845	–	848	–	624	1.36
Combination bands	–	–	~1300	–	~1300	–	~940	1.38
	–	–	1520	–	–			
ν_3	1680	1686	1680	1665	1681	1208	1222	1.38
	–	–	1770	–	–	–	–	
ν_1	1769	1763	1815 (Sh)	1730	1762	1245	1257	1.40
[AlD$_3$H]$^-$						–	1719	

Sh: shoulder.

Table 3
Infrared frequencies (ω_i in cm^{-1}) of pure NaAlH$_4$ and NaAlD$_4$ at room temperature (estimated errors ± 2 cm^{-1})

ω_i	Pure NaAlH$_4$						Pure NaAlD$_4$			Ratio (ω_i^H/ω_i^D)		
	Literature			This work			This work			This work		
	[32][a]	[31][b]	[33][a]	KBr pellet	Nujol mull	ATR	KBr pellet	Nujol mull	ATR	KBr pellet	Nujol mull	ATR
ν_2	688	–	680	690	690	–	500	–	–	1.38	–	–
	752	720	730	735	735		555	–	–	1.32	–	–
n.a.	–	800 (Sh)	–	800 (Sh)	805 (Sh)	–		–	–		–	–
ν_4	–	–	–	–	–	845	–	–	–	–	–	–
	901	910	900	900	900	895	645	640	640	1.40	1.41	–
n.a.							740	740	735			
n.a.							790	795	790			
Combination bands	–	1000 (Sh)	–	~1010 (Sh)	–	~1250 (Sh)	–	–	–	–	–	
	–	–	–	~1370 (Sh)	–	~1370 (Sh)	–	–	~1105 (Sh)	–	–	1.24
n.a.	–	–	–	–	–	–	–	–	~1150 (Sh)			
ν_3	1678	~1680	1680	1670	1675	1615	1225	1225	1210	1.37	1.37	1.33
n.a.	–	–	–	1850 (Sh)	1730 (Sh)	1730 (Sh)	–	1305 (Sh)	–	–	1.33	–
[AlD$_3$H]$^-$							1725	1725	1725			

Sh: shoulder; n.a.: unassigned bands.
[a] Nujol mull.
[b] KBr pellet.

between 680 and 900 cm^{-1}. The assignment of these lower frequency modes is not straightforward: there appear four bands at 690, 735, 800 (shoulder) and 900 cm^{-1}, while only three bands are expected ($A_u + E_u$) for ν_4, and A_u for ν_2. For these reasons, the assignments proposed in Tables 2 and 3 should be considered as tentative.

Surprisingly, the IR spectra obtained using the ATR set-up are quite different as they reveal a prominent shift of the ν_3 [AlH$_4$]$^-$ stretching band from 1670–1675 to 1615 cm^{-1}. It should be stressed that all samples were prepared in the same way. In view of our previous ATR FT-IR measurements on alkali borohydrides [18,19,34] that have always produced spectra comparable to those in the literature our sampling technique presumably did not lead to sample decomposition. There are two possible explanations for the frequency shift of ν_3:

(a) The complex permittivity at infrared frequencies of NaAlH$_4$ generates differences in ATR and transmission measurements [35].
(b) There occurs a high-pressure phase transition. High-pressure phases were theoretically predicted for NaAlH$_4$ (above 64.3 kbar [36]), experimentally found for the lithium analogue LiAlH$_4$ (tetragonal above 70 kbar and 373–673 K, and orthorhombic above 70 kbar and 773 K [37]). The latter showed a downward shift of the ν_3 [AlH$_4$]$^-$ stretching band. No such phases were observed for NaAlH$_4$ under similar conditions. Given that the samples in our ATR experiments were subjected to pressures of up to 3 kbar attempts were made to reduce the applied pressure by setting the dynamometric screw to a minimum estimated pressure of 500 bar. This value was in the upper range of typical pressures applied to prepare

KBr pellets, but afterwards the pressure was released to obtain a free pellet for IR transmission measurements. However, the only apparent effect on the spectra was a change of intensity (the higher the value of the setting, the stronger the intensity) and no frequency shift could be established.

Since neither one of these two possibilities can be excluded at present, the ATR data will be considered separately from the other IR measurements.

3.2. Milled NaAlH$_4$

3.2.1. Structure

After 40 min of milling the axial ratios and cell volumes measured at 10 K increase significantly for both the hydride (experiment No. 7: $c/a = 2.2490$, $V = 279.55$ Å^3) and the deuteride (experiment No. 9: $c/a = 2.2472$, $V = 276.79$ Å). No literature data are available for comparison as yet. Interestingly, the displacement amplitudes of the metal atoms increase by up to 30% for Na and 7% for Al ($B_{Na} = 5.6$ and 4.3 Å^2, $B_{Al} = 4.9$ and 4.6 Å^2 for milled and unmilled deuteride, respectively, and $B_{Na} = 5.1$ and 4.4 Å^2, $B_{Al} = 4.1$ and 3.9 Å^2 for milled and unmilled hydride, respectively). Furthermore, the crystallite size decrease by a factor of $\sim$2 (800 Å for milled as compared to 1700 Å for unmilled NaAlH$_4$), while the strain increases by a factor of $\sim$3 (0.59‰) for pure NaAlH$_4$; 2.16‰ for 40′ milled NaAlH$_4$ (experiment Nos. 2, 6, 7 for hydride samples and Nos. 5, 8, 9 for deuteride sample). The anisotropy of strain increases weakly in a first step and strongly after extended milling time (from an average of 0.11‰ for the three pure samples to 0.13‰ for 20′ milled and 0.25‰ for 40′ milled NaAlH$_4$).

Table 4
Infrared frequencies (ω_i, in cm^{-1}, measured with ATR FT-IR mode) of pure, milled, doped and cycled alanate samples (estimated errors ± 2 cm^{-1}); full width at half maximum (FWHM) are indicated for the ν_3 [AlH$_4$]$^-$ stretching band

	Experiment No.									
	1	6	7	10	11	12	13	14	15	16
	Sample 1 pure	Sample 2 milled 20 min	Sample 2 milled 40 min	Sample 3 doped, 2 mol% Ti(OBu^n)$_4$	Sample 1 doped, 6 mol% Ti(OBu^n)$_4$	Sample 3 doped, 2 mol% TiCl$_3$	Sample 1 doped, 6 mol% TiF$_3$	Sample 3 cycled, 2 mol% Ti(OBu^n)$_4$	Sample 3 cycled, 2 mol% TiCl$_3$	Sample 3 cycled, 2 mol% TiF$_3$
New vibration	–	710	710	710	710	710	710	705	710	700
ν_4	845	820	815	805	810	–	810	845	845	845
	895	895	895	895	895	895	895	890	890	890
Combination bands	~1250 (Sh)	~1250 (Sh)	~1250 (Sh)	~1250 (Sh)	~1250 (Sh)	~1250 (Sh)	~1250 (Sh)	–[a]	–[a]	–[a]
	~1370 (Sh)	~1370 (Sh)	~1370 (Sh)	~1370 (Sh)	~1370 (Sh)	~1370 (Sh)	~1370 (Sh)	–[a]		–[a]
ν_3	1615	1630	1635	1630	1640	1635	1635	1635	1635	1605
	~1730 (Sh)	~1730 (Sh)	~1730 (Sh)	~1730 (Sh)	~1730 (Sh)	~1730 (Sh)	~1730 (Sh)	~1730 (Sh)	~1730 (Sh)	~1730 (Sh)
FWHM of ν_3 (cm^{-1})	270	200	180	180	160	240	180	210	220	250

Sh: shoulder.

[a] Unresolved bands due to presence of vibrations from secondary phases.

3.2.2. Vibrations

The ATR FT-IR spectra shown in Fig. 2 reveal an upward shift of the ν_3 [AlH$_4$]$^-$ stretching mode from 1615 to 1635 cm^{-1} (see Table 4). In addition one notices the appearance of a new band around 710 cm^{-1}, and a downward shift of one component of the ν_4 [AlH$_4$]$^-$ bending band (from 845 to ~820 cm^{-1}) with a decrease of its intensity. At the same time the broadening of the ν_3 [AlH$_4$]$^-$ stretching line decreases by about 30% (FWHM from 270 cm^{-1} for pure NaAlH$_4$ to 200 cm^{-1} for 20′ milled NaAlH$_4$ and 180 cm^{-1} for 40′ milled NaAlH$_4$). The upward shift of the ν_3 [AlH$_4$]$^-$ stretching band presumably correlates with the observed anisotropic cell expansion on milling and the slight modification of the sodium coordination of the [AlH$_4$]$^-$ units. Similar effects, although of smaller amplitude, were observed for the milled deuteride sample (not shown here). FT-IR measurements of pure NaAlH$_4$ in KBr pellets present a similar upward displacement of the ν_3 [AlH$_4$]$^-$ stretching band upon milling (as well as upon Ti-doping) by about 15 cm^{-1} (from ca. 1670 to 1685 cm^{-1}) as in the ATR measurement.

The Raman spectra show no significant changes upon milling. Due to the reduced particle size the elastic light scattering of the samples increases, thus yielding stronger laser plasma lines and weaker Raman spectra. Line fitting analyses suggest that the position and width of the ν_3 band at 1681 cm^{-1} remains unchanged within experimental error. In principle, one would expect IR and Raman spectra to be correlated, i.e. to observe similar shifts for the ν_3 band in both experiments. The fact that this is not the case here could be related to the very broad Al–H stretching bands that suggest the presence of strong couplings with low frequency (translational?) lattice modes. This allows for the possibility that in IR and Raman experiments we do observe different components (irreducible representations) stemming from the same ν_3 vibration but coupled by symmetry to a different low frequency mode, which in turn may behave differently upon milling, including perturbations generated by strain and surface modes that become increasingly important for nanocrystalline particles.

3.3. Doped and cycled NaAlH$_4$

3.3.1. Effects of doping

Doping leads to small but significant changes in cell parameters, atomic displacement amplitudes and microstructure. The axial ratio at 10 K generally increases (up to c/a= 2.2437 for TiCl$_3$, experiment No. 12) while the cell volume decreases for Ti(OBu^n)$_4$ (experiment No. 11: $V = 278.93$ Å^3) and increases for TiF$_3$ (experiment No. 13, $V = 279.36$ Å^3) and TiCl$_3$ (experiment No. 12, $V = 279.27$ Å^3). The increase of c/a is similar to that after milling, while the decrease in cell volume for Ti(OBu^n)$_4$ doping is opposite to that after milling. Only few literature data are available for comparison, such as those reported by Brinks et al. [25] ($c/a =$ 2.2592 and $V = 287.35$ Å^3 for pure NaAlH$_4$, $c/a =$ 2.2592

and $V = 286.33\,\text{Å}^3$ for $TiCl_3$ doped hydride, $c/a= 2.2595$ and $V = 286.36\,\text{Å}^3$ for TiF_3 doped hydride from synchrotron data at room temperature), and Sun et al. [11] ($c/a = 2.2592$ and $V = 286.95\,\text{Å}^3$ for pure $NaAlH_4$, $c/a = 2.2596$–2.2634 and $V = 286.45$–$289.25\,\text{Å}^3$ for several $Ti(OBu^n)_4$ doped hydride from X-ray powder diffraction at room temperature) that show the same tendency for the axial ratio but not for the volume changes. The metal atom displacements increase as with milling but to a larger extent (14–24% for B_{Na} in doped samples compared to 16% for milled hydride, and 13–16% for B_{Al} in doped samples compared to 5% for milled hydride), while the crystallite size decreases (600–760 Å) and the strain increases (experiment Nos. 11–13: 1.6–1.8‰) similar to milling. Finally, contrary to milling, Ti-doping leads to the formation of secondary phases such as Al (up to 8 wt.%, see Table 1) which implies a partial loss of hydrogen.

The Raman spectra of the doped samples are quite similar to those of the milled samples except that the signal-to-noise ratios of the latter are significantly lower because of their grey appearance. The spectra of the $Ti(OBu^n)_4$ doped sample reveal weak bands corresponding to unreacted $Ti(OBu^n)_4$. The IR spectra which are less sensitive to colouring also show similar features as milled samples: an upward shift and sharpening of the main ν_3 $[AlH_4]^-$ stretching band (see Fig. 2 and Table 4), a downward shift of one component of the ν_4 $[AlH_4]^-$ bending band, and the appearance of a new vibration at $710\,\text{cm}^{-1}$. The $TiCl_3$-doped sample shows a surprisingly broad main ν_3 $[AlH_4]^-$ stretching band (close to the value of the pure $NaAlH_4$).

3.3.2. Effects of cycling

Cycling leads to rather heterogeneous effects with respect to structure and vibrations. While the axial ratio increases for the cycled $TiCl_3$ doped sample (experiment No. 15: $c/a = 2.2446$) and for the cycled TiF_3 doped sample (experiment No. 16: $c/a = 2.2444$), it decreases for the cycled $Ti(OBu^n)_4$ doped sample (experiment No. 14: $c/a = 2.2430$). The atomic displacement amplitudes do not much change except those of the $Ti(OBu^n)_4$-doped sample (experiment No. 14) that decrease anomalously for sodium ($B_{Na} = 3.1\,\text{Å}^2$) and increase for aluminium ($B_{Al} = 6.1\,\text{Å}^2$). As expected, the average crystallite size increases strongly for all samples (1100–1600 Å^3) and comes close to that of undoped and unmilled samples. While the strain remains relatively unchanged its anisotropy changes as a function of dopants, being not far from isotropic for $Ti(OBu^n)_4$ and rather anisotropic for $TiCl_3$ and TiF_3. The IR spectra (see Fig. 2 and Table 4) reveal a downward shift of the main ν_3 $[AlH_4]^-$ stretching band by $\sim20\,\text{cm}^{-1}$ in the TiF_3-doped sample (experiment No. 16) and a broadening of the ν_3 $[AlH_4]^-$ stretching band that is difficult to quantify because of the possible contribution of the broad ν_3 band of Na_3AlH_6 at its left shoulder. Interestingly, the IR spectra of the $Ti(OBu^n)_4$ cycled experiment No. 14 still show the presence of the unreacted dopant after the cycling process.

4. Conclusion

The present study suggests that doping $NaAlH_4$ with Ti-based catalysts and milling $NaAlH_4$ in the absence of catalysts have similar effects on its structure and dynamics vibrations. Both treatments tend to increase the axial cell parameter ratios, cell volumes, atomic displacement amplitudes and strain and to decrease grain size. They lead to IR line shifts by $\sim15\,\text{cm}^{-1}$ to higher frequencies for the ν_3 asymmetric stretching mode, and by $\sim20\,\text{cm}^{-1}$ to lower frequencies for one part of the ν_4 asymmetric bending mode, thus suggesting small structural changes in the local environment of the $[AlH_4]^-$ units. The broad ν_3 bands become sharpened which suggests a more homogeneous local environment of the $[AlH_4]^-$ units, and there appears a new vibration at $710\,\text{cm}^{-1}$. The Raman data show no such effects. The effects for the doped samples depend only little on the nature of the catalyst. The only significant difference between milling and doping is the formation of Al metal and titanium halides during the latter. Cycling leads to a general re-crystallization and a less uniform behaviour with respect to structure and vibrations. In contrast to milling and doping its effects depend on the nature of the dopants. Cycling leads to a general increase in domain size (1100–1600 Å) and to a slight decrease in strain while the strain anisotropy increases except for the $Ti(OBu^n)_4$ doped sample. The shifts of the ν_3 asymmetric stretching mode in the IR spectra of cycled samples are similar to those of the doped samples except for the TiF_3 sample that shows a decrease by $\sim30\,\text{cm}^{-1}$ compared to the uncycled samples and a decrease by $\sim10\,\text{cm}^{-1}$ compared to the pure samples. The broadening of the ν_3 mode also depends on the nature of the dopant. It is strongest for the TiF_3 sample and not visible for the $TiCl_3$ sample for which ν_3 was already quite broad after doping. Altogether these observations suggest that cycling leads to a less uniform local environment of the $[AlH_4]^-$ units. The broadening of ν_3 in particular is consistent with the presence of Ti in the local environment of some of the $[AlH_4]^-$ units. Note that such an effect is less (or not) apparent in uncycled (doped) samples. This supports the idea that titanium diffusion and some substitution into the alanate lattice does occur, in particular during cycling, and that this provides the mechanism through which Ti-doping enhances kinetics during re-crystallisation [10,12,13,38]. However, before reaching a final conclusion and a more quantitative assessment of the various effects more systematic studies of doping and cycling are needed. Such experiments are under currently way.

References

[1] B. Bogdanovic, M. Schwickardi, J. Alloys Compd. 1 (1997) 253–254.

[2] C.M. Jensen, R.A. Zidan, N. Mariels, A. Hee, C. Hagen, Int. J. Hydrogen Energy 24 (1999) 461.

[3] R.A. Zidan, S. Takara, A.G. Hee, C.M. Jensen, J. Alloys Compd. 285 (1999) 119.

[4] B. Bogdanovic, M. Felderhoff, M. Germann, M. Härtel, A. Pommerin, F. Schüth, C. Weidenthaler, B. Zibrowius, J. Alloys Compd. 350 (2003) 246.

[5] M. Fichtner, J. Engel, O. Fuhr, O. Kircher, O. Rubner, Mater. Sci. Eng. B 108 (2004) 42.

[6] J.M. Bellosta von Colbe, B. Bogdanovic, M. Felderhoff, A. Pommerin, F. Schüth, J. Alloys Compd. 370 (2004) 104.

[7] A. Zaluska, L. Zaluski, J.O. Strom-Olsen, J. Alloys Compd. 298 (2000) 125.

[8] M.P. Balogh, G.G. Tibbetts, F.E. Pinkerton, G.P. Meisner, C.H. Olk, J. Alloys Compd. 350 (2003) 136.

[9] D.L. Anton, J. Alloys Compd. (2003) 356–357.

[10] G.J. Thomas, K.J. Gross, N.Y.C. Yang, C.M. Jensen, J. Alloys Compd. 330–332 (2002) 702.

[11] D. Sun, T. Kiyobayashi, H.T. Takeshita, N. Kuriyama, C.M. Jensen, J. Alloys Compd. 337 (2002) 8.

[12] T. Kiyobayashi, S.S. Srinivasan, D. Sun, C.M. Jensen, J. Phys. Chem. A 107 (2003) 7671.

[13] J. Iniguez, T. Yildirim, T.J. Udovic, M. Sulic, C.M. Jensen, Phys. Rev. B 70 (2004) 60101.

[14] J.P. Bastide, J. El Hajri, P. Claudy, A. El Hajbi, Synth. React. Inorg. Met.-Org. Chem. 25 (7) (1995) 1037.

[15] C.M. Jensen, R.A. Zidan, US Patent 6,471,935 (2002).

[16] J.C. Bureau, Z. Amri, P. Claudy, J.M. Létoffé, Mater. Res. Bull. 24 (1989) 23.

[17] J. Huot, S. Boily, V. Guther, R. Schultz, J. Alloys Compd. 283 (1999) 304.

[18] S. Gomes, H. Hagemann, K. Yvon, J. Alloys Compd. 346 (2002) 206.

[19] H. Hagemann, S. Gomes, G. Renaudin, K. Yvon, J. Alloys Compd. 363 (2004) 126.

[20] D. Lovy, PROGRAM SPECTRAW, Version 1.40, Dépt. de Chimie Physique, University of Geneva, 1996.

[21] J. Rodriguez-Carvajal, PROGRAM Fullprof.2k, Version 2.45, Laboratoire Léon Brillouin (CEA-CNRS), France, July 2003 (Fullprof.2k manual available on http://www-llb.cea.fr/fullweb/fp2k/fp2k_divers.htm). See also J. Rodriguez-Carvajal, T. Roisnel, EPDIC-8, 23–26 May 2002. Trans. Tech. Publication Ltd., Uppsala, Sweden, Materials Science Forum 123 (2004) 443–444.

[22] E.J. Mittemeijer, P. Scardi (Eds.), Diffraction Analysis of the Microstructure of Materials' Springer Series in Materials Science, vol. 68, Springer-Verlag, Berlin, 2004.

[23] B.E. Warren, X-Ray Diffraction, Dover, New York, 1990.

[24] B.C. Hauback, H.W. Brinks, C.M. Jensen, K. Murphy, A.J. Maeland, J. Alloys Compd. 358 (2003) 142.

[25] H.W. Brinks, C.M. Jensen, S.S. Srinivasan, B.C. Hauback, D. Blanchard, K. Murphy, J. Alloys Compd. 376 (2004) 215.

[26] V. Ozolins, E.H. Majzoub, T.J. Udovic, J. Alloys Compd. 375 (2004) 1.

[27] V.K. Bel'skii, B.M. Bulychev, A.V. Golubeva, Russ. J. Inorg. Chem. 28 (1983) 1528.

[28] K.J. Gross, S. Gurthrie, S. Takara, G. Thomas, J. Alloys Compd. 297 (2000) 270.

[29] D.J. Ross, M.D. Halls, A.G. Nazri, R.F. Aroca, Chem. Phys. Lett. 388 (2004) 430.

[30] A.P. Kurbakova, L.A. Leites, V.V. Gavrilenko, Yu.N. Karaksin, L.I. Zakharkin, Spectrochim. Acta A 31 (1975) 281.

[31] J.C. Bureau, J.P. Bastide, B. Bonnetot, H. Eddaoudi, Mater. Res. Bull. 20 (1985) 93.

[32] A.E. Shirk, D.F. Shriver, J. Am. Chem. Soc. 95 (18) (1973) 5904.

[33] T.G. Adiks, V.V. Gavrilenko, L.I. Zakharkin, L.A. Ignat'eva, Z. Prikladnoi Spektroskopii 6 (6) (1967) 806.

[34] G. Renaudin, S. Gomes, H. Hagemann, L. Keller, K. Yvon, J. Alloys Compd. 375 (2004) 98.

[35] K. Yamamoto, H. Ishida, Vib. Spectrosc. 8 (1994) 1.

[36] P. Vajeeston, P. Ravindran, R. Vidya, H. Fjellvag, A. Kjekshus, Appl. Phys. Lett. 82 (14) (2003) 2257.

[37] B.M. Bulychev, V.N. Verbetskii, K.N. Semenenko, Russ. J. Inorg. Chem. 22 (11) (1977) 1611.

[38] K.J. Gross, E.H. Majzoub, S.W. Spangler, J. Alloys Compd. 423 (2003) 356–357.